5-9-1986

# Use of Electron Back Scatter Diffraction Patterns for Determination of Crystal Symmetry Elements

D. J. Dingley
*University of Bristol*

Karim Baba-Kishi
*University of Bristol*

# USE OF ELECTRON BACK SCATTER DIFFRACTION PATTERNS FOR DETERMINATION OF CRYSTAL SYMMETRY ELEMENTS

D.J.Dingley[*] and Karim Baba-Kishi

H.H.Wills Physics Laboratory
University of Bristol
Bristol BS1 8TL
England

## Abstract

The application of electron back scatter diffraction in the scanning electron microscope has been extended to the determination of crystal symmetry elements, point group and space group. The wide angular range of the patterns makes this a relatively simple task compared with equivalent analysis using electron channelling patterns, convergent beam patterns or standard x-ray methods, though the complexity of the analysis does not permit an unthinking approach. To establish the best procedure specimens from the seven crystal systems were investigated and results from the examination of the metal tin (tetragonal), and minerals zircon ($ZrSiO_4$, tetragonal) and calcite ($CaCO_3$ rhombohedral) are presented. The procedure entails determination of the crystal system from detection of rotation axes, determination of point group from the observed combinations of mirror planes and rotation axes, determination of Bravais lattice, and finally, determination of space group from the absences of lines due to screw axes and glide planes. Considerable computational aids were required in the latter stages of analysis and for this a computer program was written to simulate the diffraction patterns from any crystal system and Bravais lattice with line delete procedures to remove lines forbidden because of space group requirements.

*Address for correspondence:
D.J.Dingley, University of Bristol,
H.H.Wills Physics Laboratory,
Royal Fort, Tyndall Avenue,
Bristol, BS8 1TL, UK Tel. 0272 303030

## Introduction

X-ray diffraction is still the most widely used technique for the complete determination of crystal structure, electron diffraction, by comparison, giving for the most part, poorer information. However, the recent work of Steeds and co-workers (2,12) using convergent beam techniques in the transmission electron microscope, has considerably advanced the use of electron diffraction for this purpose. No equivalent work has yet been published on analysis of diffraction patterns obtained in the scanning electron microscope, (SEM). However, the wide angular range of the diffraction patterns obtained in the SEM using Venables and Harland's technique (13), suggests that such analysis should be applicable in this case.

The development of Venables and Harland's diffraction technique, which is essentially a method for obtaining wide angle back scattered Kikuchi patterns, can be traced through the papers of Venables and co-workers (7,8,13-16), Dingley and co-workers (4-6), and more recently Bennett and Pickering (1) and Reimer et al (9-11). It has been reviewed and compared with the more common technique, selected area electron channelling, by Dingley (3). In Dingley's modification of Venable's original method (6) considerably improved detail in the patterns was obtained by recording them directly on photographic film placed in the vacuum of the microscope specimen chamber. The quality of these photographs indicated that they could be used for identification of crystal symmetry elements with point group and space group determination. This paper describes the analytical techniques developed to do this.

It was found that the patterns were too complex and varied to be able to prescribe a unique method of analysis. Rather, different approaches had to be successively tried and abandoned if a subsequently drawn computer simulation of the pattern did not match the experimental perfectly. The methods adopted are reported here with reference to the analysis of β-tin (tetragonal), zircon ($ZrSiO_4$, tetragonal) and calcite ($CaCO_3$, rhombohedral) with respective space groups $I4_1/amd$, $I4_1/amd$ and $R\bar{3}2/c$.

The following description of experimental

procedure is kept brief and limited to details of specimen preparation, computer simulation and methods of data acquisition from the photographs. A detailed account of the electron back scatter diffraction technique itself can be found in the references quoted above, particularly ref.4.

## Experimental

### Specimen preparation

The electron back scatter diffraction technique requires the specimen surface over the area from which the pattern is generated, to be flat, reasonably strain free and free of contamination or other surface films. However, as this area extends little beyond the diameter of the incident beam (8,4), i.e typically less than 100nm, such favourable areas could be found even in quite macroscopically rough specimens. Thus in examining the mineralogical specimens Zircon and Calcite use could be made of their natural growth or cleavage facets and no mechanical or chemical polishing was required. They were cleaned prior to examination in an ultrasonic bath containing a commercial degreasing agent, 'Arklone' and were necessarily examined uncoated as it had been shown earlier, (4) that as little as 5nm of a metallic film deposited over the surface to prevent charging in the SEM, caused the diffraction patterns to become extremely diffuse and obscure. The consequent charging had still to be minimised by other means however, as this also affected the quality of the resulting patterns. It was found useful to operate at as low a beam voltage as possible, though, 15kV was the minimum practicable when recording directly on standard electron microscope film. If the specimen was small it was found helpful to embed it in a soft metal such as indium or a gold film deposited on a plastic base. This left only a small area of non conducting material exposed and a reasonably stationary probe could be produced for the 10 sec exposure time required.

The preparation of the 10mm diameter β-tin sample followed standard metallographic grinding and lapping procedures followed by electropolishing in Strurers A2-1 electrolyte for 30s. at a current of 1.8amps. To prevent the normally rapid surface oxidation of this specimen it was kept under 'Arklone' solvent and examined in the SEM as soon after preparation as possible.

### Electron microscopy

The samples were examined in a Cambridge Instruments S4 'Stereoscan'to which a sheet film camera had been attached to enable the electron back scattering patterns to be recorded. The patterns were obtained with the beam focused as a stationary probe on the selected area and were imaged on a phosphor screen placed 40mm in front of the specimen which was in turn viewed using a low light television camera. The television camera type was a Mullard 'intensified silicon intensified target (ISIT) camera.' The arrangement is shown schematically in Fig.1 and is described in detail in ref.4. The normal operational conditions were:- specimen current to provide a clear image at a gain of $10^5$ on the ISIT camera, 0.1nA, accelerating voltage,15-30 kV, exposure

time at the above specimen current and using Ilford special contrasty electron microscope film, 10s., angular range covered by the diffraction pattern 90°. The specimen was tilted towards the screen by up to 70° from the horizontal. Adjustments to tilt and rotate controls were then made to bring the required part of the diffraction pattern into view. However, because of the large angular range of the recorded patterns two or three patterns only were needed to cover a sufficient fraction of reciprocal space. Patterns were recorded from the different cleavage and growth faces of the mineralogical specimens and several patterns from individual crystals in the polycrystalline tin sample. These are presented below.

### Interrogation of diffraction patterns

The data required to be determined from the diffraction patterns were lattice spacing d, angles between zone axes θ, and angles between crystal planes β. Such measurements require a knowledge of the pattern centre, PC, and the specimen to film distance Z. Determination of the latter parameters has always been difficult and several techniques have been reported, (4,15) for their measurement. The method used in these investigations was that briefly mentioned in ref.4, where these parameters are found by calibration using a specimen of known orientation.

### Determination of pattern centre and specimen to film distance

Prior to recording a set of diffraction patterns a cleaved 5mm square single crystal silicon wafer was mounted in the microscope on a chamfered specimen stub. The surface normal of the crystal was [001]. One of the cleaved edges, which lie along [110], was set parallel to the horizontal. With the specimen stage set against stops at the zero tilt and rotate positions the crystal surface normal faced the screen directly and was inclined at an angle 19.4° with respect to the incident beam. The silicon crystal was thus set at an orientation such that the [011] direction lay in the plane defined by the direction of the incident beam and [001]. This arrangement ensured accurate alignment of the [114] crystal direction normal to the recording (or viewing) plane, so defining the position of the pattern centre. It also ensured that the [111] zone axis lay vertically below it so defining the vertical axis of the system. These zone axes are marked in Fig.2 which is an example of one of the calibration pictures used in the present study. The specimen to film distance was obtained from measurement of the distance between the [114] and [111] zone axes on the diffraction pattern, and using the formula:

$$Z=L/(\tan(35)) \qquad (1)$$

where 35° is the angle between the [114] and [111] directions in silicon. This method gave the pattern centre and specimen to film distance an accuracy of 0.5% which was of the same order as the accuracy of other measurements that could be made in the diffraction patterns.

In order to be able to relocate the pattern

centre in subsequent photographs the coordinates of the pattern centre were measured with respect to fiducial shadows cast by two pins. These shadows are labelled S,S in Fig.2. The pins were firmly attached to the camera assembly so that their shadows were always in the same absolute position with respect to the pattern centre in all photographs. The method also required however, that the focused specimen was always at the same height and the electron beam positioned at the same lateral settings in each photograph. Repetition of lateral setting was achieved by working at high magnification and switching off the electromagnetic beam shift controls. Constancy in specimen height was achieved by maintaining the objective lens setting at a fixed value and focusing specimens using the specimen height shift control. The error introduced by these constraints was less than the 0.5% error in determining the pattern centre.

Determination of lattice spacing

Lattice spacings were determined by measuring the angle $\Delta\theta$ Fig.3, across a pair of Kikuchi lines. This equals twice the Bragg angle. As the projection is gnomonic, the measurement was made along the radius normal to the Kikuchi band, where the radius is drawn from the pattern centre. The d spacing was then given by

$$d = \lambda /(2 \times \sin(0.5(\theta'' - \theta'))) \qquad (2)$$

$$\theta'' = \arctan((r+r')/z), \quad \theta' = \arctan(r'/z)$$

where r,r' are as defined in the figure and where $\lambda$ is the wavelength of the radiation. The accuracy of such measurements was not high, 4%. It was determined principally by the diffuse width of the Kikuchi lines.

Determination of angles between zone axes, (interzonal angles)

The angle between two zone axes, such as A,B in Fig.2, was found by determining the coordinates (xy)A (xy)B of each of the axes with respect to the pattern centre so allowing the zone axis vectors $\underset{\sim}{A}=(xyz)A$, $\underset{\sim}{B}=(xyz)$ to be defined. The inter axes angle was then given by calculating the inverse cosine of the scalar product of the two vectors. The accuracy of these measurements can be assessed from table 1 which shows the measured and theoretical interzonal angles determined in Fig.2. It is seen to be considerably better than 0.5°.

Determination of angles between crystal planes, (interplane angles)

The angle $\beta$ measured between a pair of Kikuchi bands, such as AN NB in Fig.2, does not necessarily equal the angle between the corresponding crystal planes. This is because of the distortion introduced by the gnomonic projection. The true interplane angles were obtained by determining the coordinates, with respect to the pattern centre, of two points on each band with one of the points common to both, eg., N. The vectors $\underset{\sim}{A}$, $\underset{\sim}{B}$, $\underset{\sim}{N}$ were then obtained as previously, the vector products $\underset{\sim}{A}x\underset{\sim}{N}$ and $\underset{\sim}{B}x\underset{\sim}{N}$ were calculated to give the vectors normal to the planes from which the interplane angles could be obtained by determining the inverse cosine of
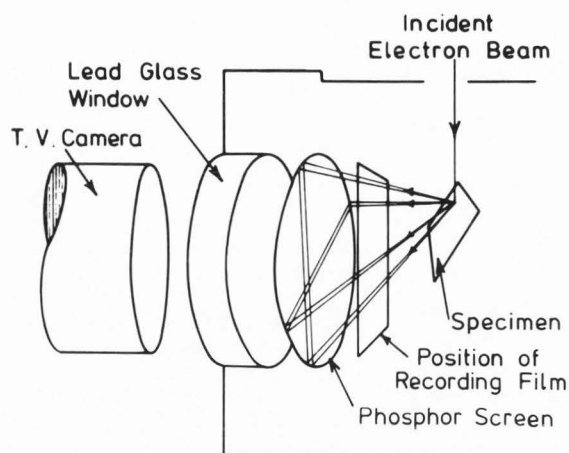


Fig 1 Schematic diagram illustrating arrangement of phosphor screen and TV camera for detecting EBSPs.
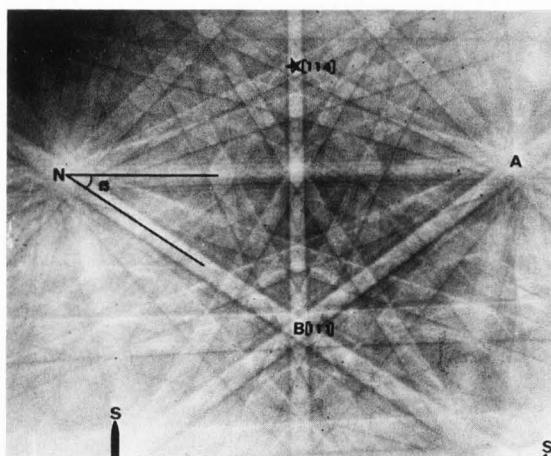


Fig 2 EBSP from silicon; used for calibration purposes. A and N are [011] and [101] poles respectively.
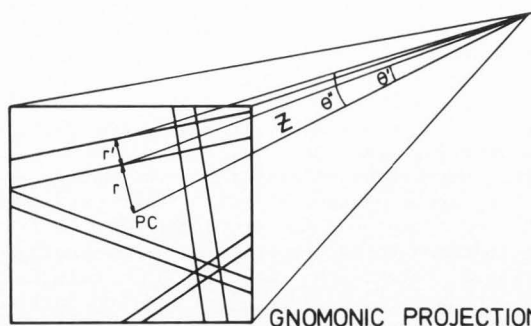


Fig 3 Schematic diagram showing construction for calculating Bragg angle from EBSPs.
PC = pattern centre. Z = specimen to film distance

their scalar product. The accuracy of the measurements can again be assessed by reference to table 1. It is seen to be of the order 1°.

## Table 1

Measured and theoretical angles between zone axes in Fig.2.

| 1st Z.A | 2nd Z.A | measured | theoretical |
|---------|---------|----------|-------------|
| 011(N) | 101(A) | 59.4 | 60 |
| 011 | 111 | 35.1 | 35.4 |
| 111 | 112 | 19.4 | 19.5 |
| 112 | 121 | 33.0 | 33.3 |

Measured and theoretical angles between crystal planes in Fig.2.

| 1st pln | 2nd pln | measured | theoretical |
|---------|---------|----------|-------------|
| 011(N,B) | 101(B,A) | 119.9 | 120 |
| 011 | 110(B,*) | 60.9 | 60 |
| 111 | 101 | 35.4 | 35.1 |
| 111 | 110 | 88.9 | 90 |

### Digitising of diffraction patterns

The above measurements were carried out either "on-line" using the directly displayed image from the ISIT television camera, or from prints of the diffraction patterns photographed directly in the specimen chamber. The on-line measurements are described elsewhere. The measurements from prints were conducted using a digitising table coupled to a microcomputer. The accuracy of the table was 0.2mm in 400mm. Its design was based on that of a pantograph machine where the coordinates of a selected point are determined from the angular deviations of the two arms of the pantograph from their home positions. Two linear servo potentiometers were mounted at the link points of the arms and the offset voltage read through an analogue to digital converter into a BBC microcomputer. A calibration curve, produced for each potentiometer, permitted correction of any non-linearity through a look-up table. Sampling speed was 1ms. with the average of 500 readings being taken when a data point was to be stored.

### Results

Out of the several sets of electron back scattering patterns (EBSPs) recorded from the tin, zircon and calcite specimens a montage from each set was compiled to depict in a single picture a large angular coverage of reciprocal space. An example is shown in Fig. 4a. The angular range of the combined patterns exceeded 140° in all cases. The pattern centres in each pattern are marked by asterisks.

In order to establish the principles by which such patterns could be interrogated to deduce the crystal symmetry we proceeded as though the samples were of unknown structure. It became clear that there were many approaches and that a completely mechanical and unthinking analysis was not possible. At some stage guessed solutions needed to be tested against computer simulations

of the diffraction patterns. The computer program used was written in basic for a BBC 1.2 microcomputer with 32k bytes of memory. Considerable flexibility in the program was found necessary to enable simulation of patterns from any crystal system, Bravais lattice or crystal orientation with the ability to alter the crystallographic parameters, add to or delete lines from the patterns, to magnify details and to interrogate the patterns to provide the index of any selected zone axis, the angle between selected zone axes or angles between crystal planes. Permanent records of the plotted patterns were obtained by photographing the display monitor, by a screen dump onto a dot matrix printer or through a digital graph plotter.

### Analysis of EBSPs from tin

The diffraction patterns shown in Fig.4a were first examined to discover the presence of all mirrors and rotation axes. The mirrors found are labelled aa', bb', cc', dd' ee'. The distortion produced by the gnomonic projection destroys perfect reflection symmetry across the mirrors in the diffraction patterns. However, the resulting pseudo symmetry can be detected with experience. As an illustration features ll', mm', nn' are reflections across the mirror aa'. The mirror ee' has no strong Kikuchi band running along it. Features pp', qq' reflected across it indicate its presence.

The intersection of mirrors aa', bb', cc', dd' at a point identify the zone axis A as a tetrad axis and the intersection of mirrors ee' with aa' and ee' with dd', identify zone axes B and C respectively, as diads. The angles between zone axes A B, between A C and between B C were 90°, 90° and 45° respectively and the angles between the crystal planes defined by the Kikuchi bands aa' and ee' and between dd' and ee' were both 90°. From these observations the point group can be identified as 4/mmm and hence the crystal system is tetragonal.

The zone axis A must have indices [001] but B and C could be either of [010] or [110]. At this point it is not possible to decide between the alternatives. If the Bravais lattice were known and there were no missing reflections due to glide planes or screw axes, then the indices of the narrowest Kikuchi band visible aa' which corresponds to the lowest order reflection, could have been identified. For the lowest order reflection for a primitive lattice is (100) for a body centred lattice (110) and for a face centred lattice (111). However, without foreknowledge of the Bravais lattice it is not possible to proceed in this way. It was decided therefore to determine first, the lattice parameter ratio a:c. Again, because of the uncertainty as to Bravais lattice and any missing lines, attempts to obtain this ratio from the measured ratio of d spacings of the Kikuchi bands bb' and ee' or for bands cc' and ee' etc., made little headway. The best procedure was to determine the ratio a:c by measurement of interzonal angles. This required a certain amount of initial guesswork and deduction. The arguments were as follows. If aa' was the (100) Kikuchi band then the major zone axes that appear between A and B along it would be, and in
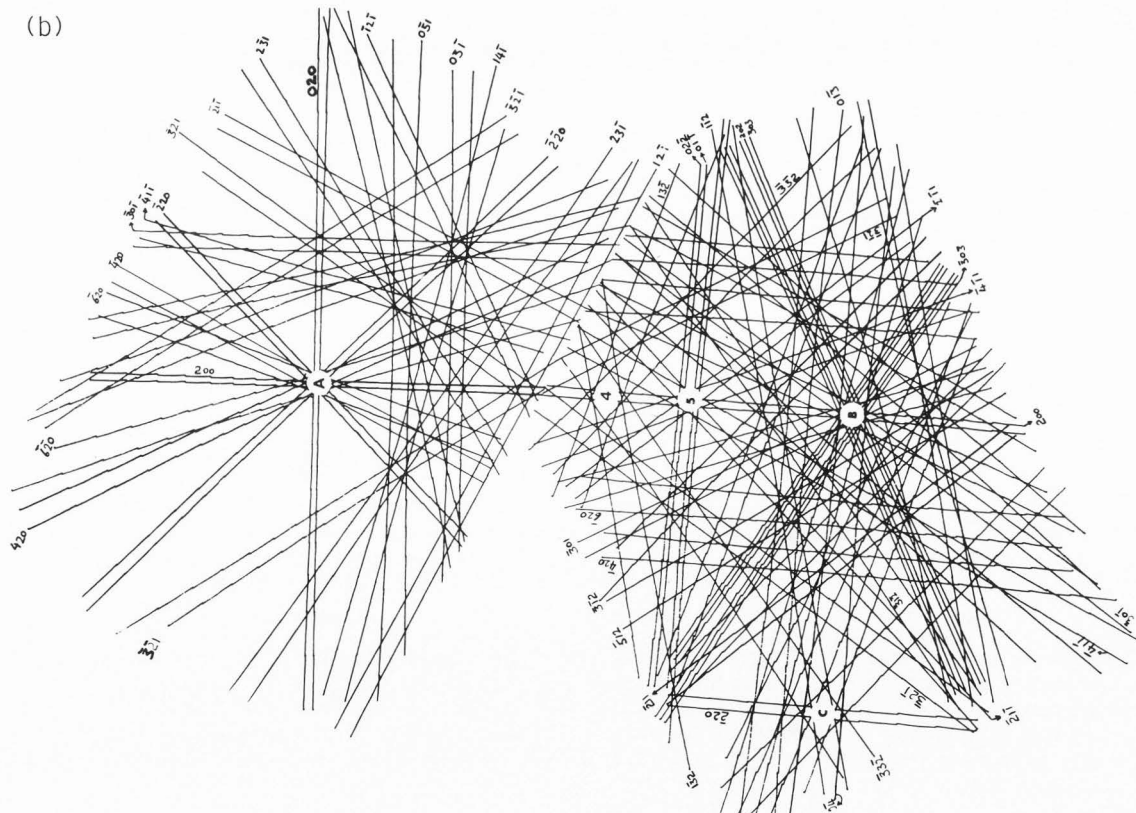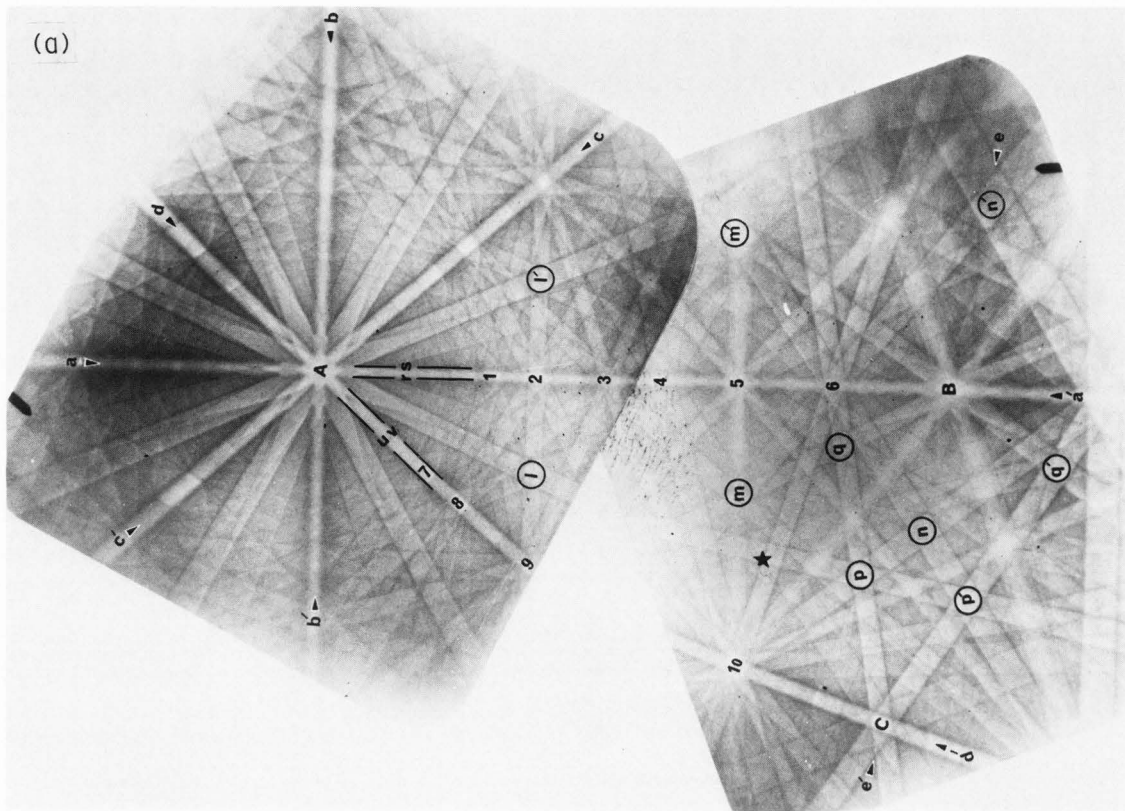
Fig. 4a: Montage of two EBSPs from β tin with prominent zone axes marked.  Fig. 4b: Computer drawn map of Kikuchi lines corresponding to the β tin EBSPs shown in Fig. 4a.

order from [001]; [013], [012], [023], [011], [032], [021] and [031]. Not all of these would necessarily be clearly distinguished. Likewise if dd' was the (110) band then the major axes along it from [001] would be [117], [115], [113], [112], [111], [221] and [331]. The converse would be true if aa' was the (110) band and dd' the (100) band. We guessed that the first option was true and made a guess also as to which of the zone axes 1 to 6 in Fig. 4a was [011]. For any such guess the a:c ratio was given by

$$a/c = \arctan\phi \qquad (3)$$

where $\phi$ is the measured angle between [001] and the guessed [011] zone axis. As the angles between all other zone axes along aa' dd' are unique to the a/c ratio calculated it was possible to test if the original guess was correct by comparing the subsequently calculated angles with the measured angles. Table 2 shows the results of such trials.

## Table 2

Measured and calculated angles between [001] and zone axes R in Fig.4 for β tin

| Zone R | measured Angle | calculated angles for axes R guessed to be [011] | | |
|---|---|---|---|---|
| | | R=9 | R=4 | R=5 |
| 1 | 23 | 26.4(117) | 22.4(013) | 24.7(014) |
| 2 | 32 | 35 (115) | 31.7(012) | 31.1(013) |
| 3 | 42 | – – | 39.5(023) | 42.1(012) |
| 4 | 51 | 49.4(113) | 51 (011) | 50.3(023) |
| 5 | 61 | 60.3(112) | 61.7(032) | 61 (011) |
| 6 | 74.5 | 74.1(111) | 74.9(031) | 74.6(021) |
| 7 | 28 | 26.4(015) | 30.2(113) | 27 (115) |
| 8 | 40.5 | 39.5(013) | 41.2(112) | 40.4(113) |
| 9 | 53 | 51 (012) | 60 (111) | 52 (112) |
| 10 | 68 | 68 (011) | 74 (221) | 68.6(111) |

It was unambiguously concluded that aa' was in fact the (100) band and dd' the (110), with a:c= 0.55. At this stage it was still impossible to distinguish whether the Kikuchi lines seen along aa' dd' were first order, second order etc.. We assumed first that they were first order. It followed then that as the band aa was the narrowest, then the Bravais lattice must be primitive. (This was shown later to be incorrect as a screw axis along [001] renders the first order reflection invisible. Nevertheless, we proceed as though our deductions were correct in order to demonstrate the complete analytical procedures.)

The Kikuchi lines rs were thus indexed as (100), ($\bar{1}$00) and from their separation the lattice parameter, a, was calculated as 0.3nm. Kikuchi lines u v were consequently indexed as (110) and ($\bar{1}\bar{1}$0). Sufficient information was then known to produce a computer drawn simulation of the pattern. The first simulation was drawn with the [001] zone axis positioned at the pattern centre, the resulting pattern compared with the experimental, and tilting and rotating operations

performed till the two patterns matched in orientation, Fig.4b In practice only a few lines were simulated at a time as too many confused the problem of identification. Small areas were simulated in detail as in Fig.5a which shows the intersection of ($1\bar{4}1$), ($14\bar{1}$), ($2\bar{3}1$), ($23\bar{1}$) and ($03\bar{1}$) lines. When compared with the same area of the experimentally obtained pattern, Fig.5b, differences are apparent. The simulated ($1\bar{4}1$) band is twice as wide as that observed experimentally. Thus as $1\bar{4}1$ is the lowest order reflection of its type, the simulated band is the narrowest possible and the only reason why the experimental band can appear narrower is because the original value of the lattice parameter was too small. It follows that Kikuchi lines rs must have been higher order than (100). Re-indexing them as (200) ($\bar{2}$00) and u v as (220) ($\bar{2}\bar{2}$0) gave a value for, a, of 0.58nm. A new simulation was produced which gave a perfect fit with the experimental pattern as can be seen in Fig.5c.

In order to next establish the Bravais lattice a comprehensive comparison between predicted lines for each lattice and observed lines was necessary. Table 3 details the comparison. From this it is evident that the fit is far better for a body centred lattice than for either a primitive or face centred lattice.

Such a list of course also provides the information needed to deduce the space group. It is seen that the conditions for visibility of lines are: h+k+l=2n, for lines hhl 2h+l=4n. For lines hk0, h or k=2n and for lines 001, l=4n. From standard tables it is seen that these data confirm the body centred Bravais lattice and establish the presence of glide planes 'd' and 'a' parallel to (110) and (001) respectively and also the presence of a $4_1$ screw axis along [001].

## Table 3

Observed and absent reflections in Fig.4 for β tin

| Class | observed reflection | absent reflection | condition observed | cause |
|---|---|---|---|---|
| hkl | 200,020,400 040 204,$\bar{2}$04,420 031,301,013 | 010,100,00$\bar{1}$ 030,300 111,333 | h+k+l=2n | I lattice |
| hhl | 22$\bar{4}$,224,2$\bar{2}$4 11$\bar{2}$,112,1$\bar{1}$2 $\bar{1}$16,$\bar{1}$16,116 | 1$\bar{1}$0,110 | h+k+l=2n 2h+l=4n | diamond glide (110) |
| hko | $\underline{6}$20,$\overline{6}$20,$\overline{4}$20 $\overline{4}$20 | $\overline{3}\overline{1}$0,$\overline{3}$10,$\overline{2}\overline{1}$0 2$\overline{1}$0 | h+k+l=2n h=2n k=2n | axial glide (001) |
| okl | 011,02$\underline{2}$,031 013,01$\bar{3}$ | – – – | h+k+l=2n | |
| 001 | 00$\overline{4}$ | 00$\bar{1}$,002,00$\bar{3}$ | h+k+l=2n l=4n | $4_1$ screw axis |

## Zircon

The analysis of the diffraction patterns from zircon Fig.6 proceeded as for tin. Mirror planes were first identified with zone axes A B and C being identified as tetrad and two diads respectively. B and C were 90° from A and 45° apart. Again the structure is seen to be tetragonal with point group 4/mmm. The interzonal angles were measured and are listed in table 4. When zone axis 3 was guessed as being [001] on the (h00) band a comparison between calculated and observed interaxes angles was found to be within experimental error, see table 4. The patterns were indexed accordingly. The same procedure as for tin was then adopted to establish the Bravais lattice and again the lowest order reflections (100) (110) were found to be missing. Kikuchi lines rs uv were found to be (200), ($\bar{2}$00), (220) and ($\bar{2}\bar{2}$0) respectively with lattice parameters a=0.64nm and c=0.57nm. From the list of observed and absent reflections the Bravais lattice was again seen to be body centred and the space group as before, I41/amd.

### Table 4

Measured and calculated angles between [001] and zone axes R in Fig.6, for zircon

| Zone R | measured Angle | calculated angles for axes R guessed to be [011] | | |
|--------|----------------|---------|---------|---------|
| | | R=7 | R=2 | R=3 |
| 1 | 19.5 | 18.7(117) | 20.3(012) | 19.6(013) |
| 2 | 36.5 | 38 (113) | 36.5(101) | 35.5(023) |
| 3 | 47 | 49.6(112) | 47.9(023) | 47 (011) |
| 4 | 65 | 67 (111) | 65.7(031) | 65 (021) |
| 5 | 27.5 | 29 (013) | 27.6(112) | 26.8(113) |
| 6 | 38.5 | 39.7(012) | 46.3(111) | 37.1(112) |
| 7 | 59 | 59 (015) | 64.4(221) | 56.5(111) |

## Calcite

The dominant feature of the diffraction pattern from calcite, Fig.7 is the triad axis A located at the intersection of the three mirror planes aa', bb' and cc'. The point labelled F lies 54.5 degrees from the triad A. If the structure had been cubic a tetrad axis should have been observed at this point. The absence of any zone axis here thus eliminates the cubic possibility. The crystal is therefore rhombohedral. There are five possible point groups for this system 3, $\bar{3}$, 3m, 32, and $\bar{3}$m. To distinguish 3 and $\bar{3}$ it was necessary to view the area of the pattern 90° to the triad, i.e., along the band dd'. We noted that features such as m,m' are identical but inverted across dd' and rotated about the triad by 60°. This corresponds to $\bar{3}$. It followed that because of the mirrors aa' etc., then zone axes B C had to be rotation diads as inspection indeed showed. The point group of the system must therefore be $\bar{3}$m. The Zone axes A B C could then be indexed as [111], [2$\bar{1}\bar{1}$] and [1$\bar{1}$0] and the bands aa' as (01$\bar{1}$), bb' as (10$\bar{1}$) and dd' as (111). This time there are no problems in making these deductions without recourse to calculation of interzonal angles, as the rotation diads must have indices of the [110] type. To
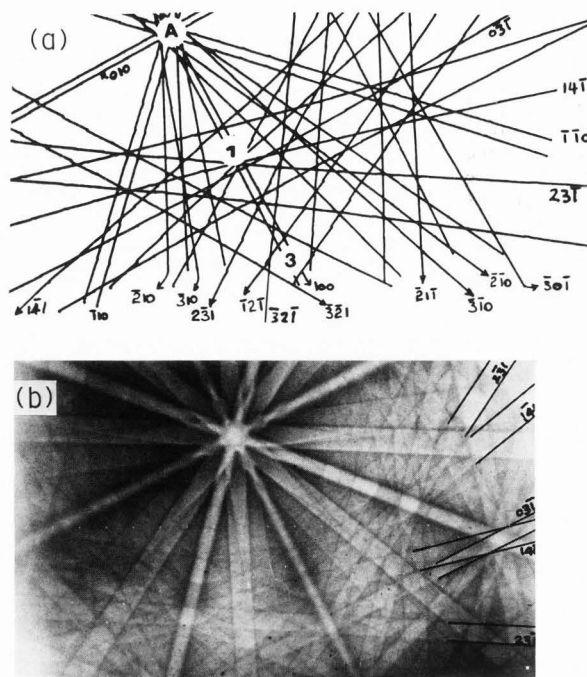


Fig 5 a) Detail of computer simulation for β tin with a = 0.3 nm, a:c = 0.554.
   b) Detail of EBSP from β tin with a = 0.58, a:c = 0.554.
   c) Detail of computer simulation for β tin with a = 0.58, a:c = 0.554.

label other zones however, the guessing procedure adopted previously was carried out. The zone axes 1-6 on the (01$\bar{1}$) band have indices amongst and in the order, [31$\bar{1}$], [611], [100], [7$\bar{1}\bar{1}$], [6$\bar{1}\bar{1}$], [5$\bar{1}\bar{1}$] and [2$\bar{1}\bar{1}$]. The comparison between calculated and measured angles which gave the best match, table 5, indicated zone axis 3 was [100]. The angle between zone axes 3 and 7, i.e., between [100] and [001] was measured as 46°. This is the angle a needed to define the rombohedral lattice. Only the primitive lattice is possible in this crystal system so that the computer simulation of the diffraction pattern could be drawn immediately. Inspection as before for missing lines showed that all orders of hkl were present. The absence of the hhl class of reflections except for l=2n indicates the presence of a c glide plane parallel to (110). This identified the space group as R$\bar{3}$2/c.

### Conclusions

The above results and analysis demonstrate

both that the electron back scattering diffraction technique can yield information suitable for detailed crystallographic analysis and that the analysis itself though complicated is unambiguous. Similar analysis has been carried out on a variety of materials covering the seven crystal systems and including metals semiconductors and further minerals. It has also been used for the identification of unknown structures the results of which will be published shortly.

## TABLE 5

Measured and calculated angles between [111] and zone axes R in Fig. 7 for calcite.

| Zone R | Measured angle | Best fit of calculated angle assuming R=3 |
|---|---|---|
| 1 | 12 | 11.2(311) |
| 2 | 16.5 | 15.7(611) |
| 3 | 28.5 | 27.0(100) |
| 4 | 47.5 | 45.5(511) |
| 5 | 65.5 | 63.8(311) |
| 6 | 91.0 | 90 (211) |

## Acknowledgements

## References

1. Bennett BW, Pickering HW, (1984) A scanning electron microscope stage for crystal orientation and structure determination. Scripta Met. 18 743-748.
2. Buxton BF, Eades JA, Steeds JW, Rackham GM, (1976) The symmetry of electron diffraction zone axis patterns, Phil. Trans. 281 171-194.
3. Dingley DJ, (1981) A comparison of diffraction techniques for the SEM. Scanning Electron Microsc.1981; IV:273-286, 258.
4. Dingley DJ, (1984) Diffraction from sub-micron areas using electron backscattering in a scanning electron microscope. Scanning Electron Microsc. 1984; II: 569-575.
5. Dingley DJ, Burns G, (1984) Diffraction studies of laser annealed silicon, Inst. of Phys. Conf. Series No. 68 Inst. of Physics. Bristol London 433-436.
6. Dingley DJ, Baker L, Hunnings L, (1981) EBSPs from semiconductor materials. Inst. of Phys. Conf. Series No. 61 Inst. of Physics. Bristol London 541-544.
7. Harland CJ, Klein JH, Akhter P, Venables JA, (1978) Electron backscattering patterns in a field emission gun SEM; In: Proc. 9th. Int. Conf. on Electron Microscopy, J M Sturges, (ed.) Microscopical Soc. of Canada, Toronto, 564-565.
8. Harland CJ, Akhter P, Venables JA, (1981) Accurate microcrystallography at high spatial resolution using EBSP in a field emission gun SEM, J.Phys. E. 14 175-182.
9. Reimer L, Popper W, Brocker W, (1978) Experiments with a small solid state detector for BSE. Scanning Electron Microsc. 1978; I: 705-710.
10. Reimer L (1984) Electron signal and detector strategy. In: Electron Beam Interactions With Solids, Eds. D.F. Kyser, H. Niedrig, D.E. Newbury, R. Shimizu. SEM, Inc., AMF O'Hare, IL. 299-310.
11. Reimer L, Popper W, Volbert B, (1977) Contrast reversals in the Kikuchi bands of backscattered and transmitted EDPs. Inst. of Phys. Conf. Series No. 36. DL Misell (ed.) Inst. of Physics. Bristol and London 259-262.
12. Steeds J W (1979) Convergent beam electron diffraction, In: Introduction to analytical electron microscopy, JI Goldstein, DC Joy (eds) Plenum Press New York and London 387-422.
13. Venables JA Harland CJ, (1973) Electron backscatter patterns- a new technique for obtaining crystallographic information in the SEM, Phil. Mag. 27 1193-1200.
14. Venables JA, Harland CJ and Akhter P, (1976) Accurate microcrystallography in the SEM; In: Proc. 38th annual meeting EMSA, Claitor's Publ. Div., Baton Rouge, LA, 184-187.
15.Venables JA, Harland CJ, Bin-Jaya R, (1976) Crystallographic orientation determination in the SEM using electron backscatter diffraction patterns and channel plates; In: Developments in electron microscopy and analysis, Academic Press London 101-104.
16.Venables JA, Bin-Jaya R, (1977) Accurate microcrystallography using EBSPs, Phil. Mag. 35 1317-1321.

## Discussion with Reviewers

JM Cowley: Since the back scattering diffraction patterns are generated by dynamical diffraction processes, one might expect that the indications of crystal symmetry might follow those of other dynamical diffraction effects such as those in convergent beam electron diffraction (CBED). Is this so? In particular is it possible to deduce the presence or absence of a centre of inversion from these patterns, and do upper layer line effects provide evidence of three dimensional symmetry relationships?

Authors: Yes, EBSP diffraction is essentially a dynamical event so one might use the same principles of interpretation as used in CBED. However, the effects are weaker and difficult in many cases to see. For example, superlattice reflections seen easily in transmission electron microscopy are not seen at all in EBSPs. Dynamical effects at the intersection of Kikuchi lines are readily seen though, so that in favourable cases it may be possible to deduce inversion centres through such means. Normally, the whole pattern is inspected to reveal the symmetry. This utilises the upper layer lines and an illustration of the application of such techniques to discover an inversion centre is given in the text in the analysis of EBSPs from calcite.

JM Cowley: It should, in principle, be possible to derive indications of systematic absences just from the configuration of lines around the main axial directions since the array of lines about any pole has an inverse relationship with the array of spots in zone axis patterns. Is this feasible in practice?
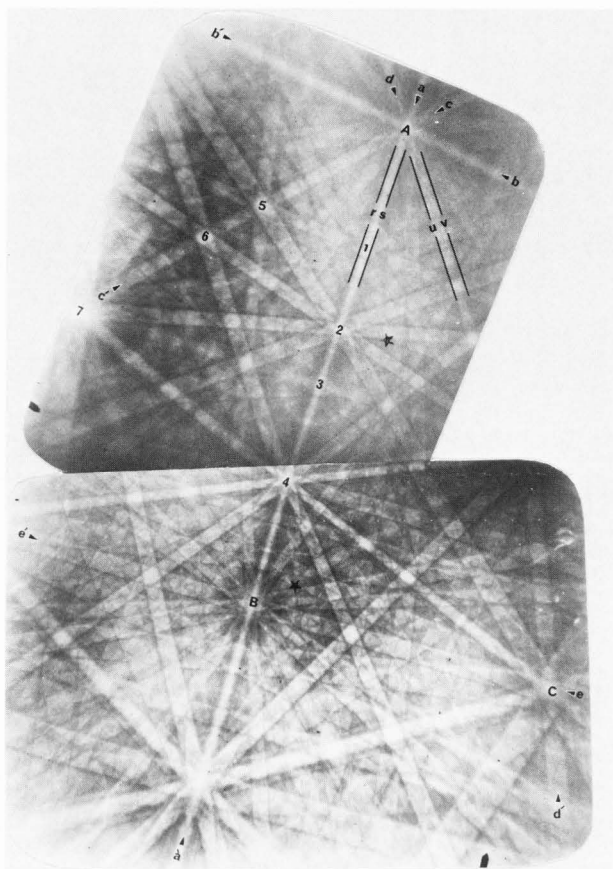
Fig 6   Montage of two EBSPs from zircon with
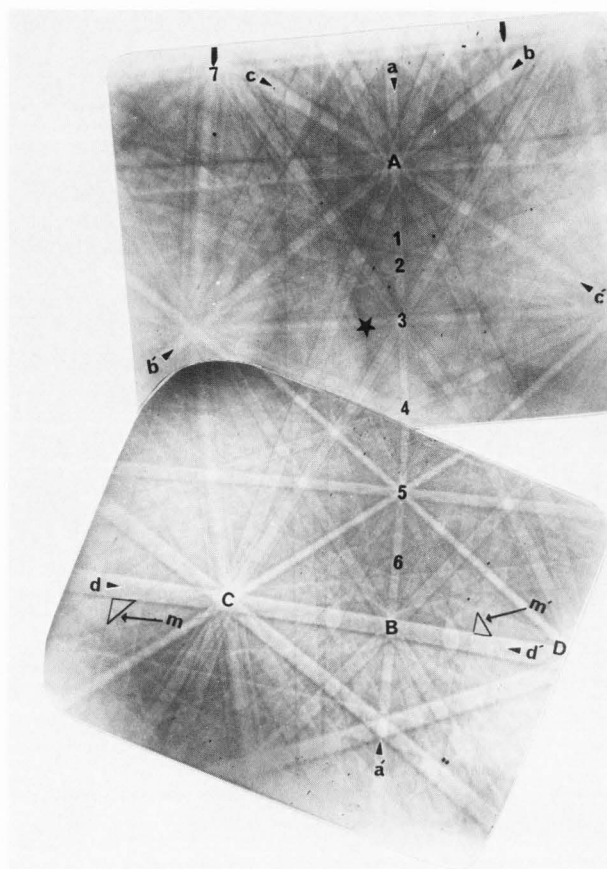        principal zone axes marked.



Fig 7   Montage of two EBSPs from calcite with
        principal zone axes marked.

Authors: Yes, it is the procedure attempted first. As the patterns are wide angle however, additional information as regards the origin of the absences can be obtained by inspection at angles 90° from a zone axes. It is the large angular range of the patterns that makes them particularly useful.

DL Davidson: On irregular specimens how is the angle of tilt known?
Authors: The interpretation of the EBSPs does not depend on a knowledge of the tilt of the crystal examined. It is only necessary to know the pattern centre and the specimen to film distance. If the orientation of a particular face of a crystal with respect to the diffraction pattern is needed, then the orientation of this face could be determined by first arranging the crystal to lie parallel to the recording plane and then tilting through a known angle till a pattern was seen on the screen.

DL Davidson: On irregular specimens, how is the specimen to film distance known?
Authors: The specimen to film distance is determined from the calibration specimen. It is equal to the distance from the point at which the incident electron beam strikes the crystal to the recording screen. As this point is fixed in space as the point along the optic axis of the

microscope where the beam is focused, it is independent of the sample orientation. Thus specimens to be examined are always brought into focus using the specimen height shift control with the beam tilt controls centred.

DL Davidson: The analysis technique seems complex; it may be used only on crystals having virtually no deformation. Is this technique likely to be particularly useful?
Authors: The technique is no more complicated than any crystallographic procedure that can yield such detailed information. The examples chosen were selected specifically to illustrate the varied types of specimen on which it can be used. When compared with x-ray powder techniques or convergent beam electron diffraction it can be a far quicker method giving less ambiguous information than the former and requiring far less specimen preparation than the latter. We have used it on metals, minerals and ceramics.

DL Davidson: Is a copy of your computer program for simulating patterns published or otherwise available?
Authors: The program has not been published but it can be obtained from Agar Aids Limited, 66A Cambridge Rd., Stansted, Essex CM24 8DA, United Kingdom.